

Received July 7, 2020, accepted July 22, 2020, date of publication July 27, 2020, date of current version August 7, 2020.

Digital Object Identifier 10.1109/ACCESS.2020.3012088

# Intelligent Adaptive Jerk Control With Dynamic Compensation Gain for Permanent Magnet Linear Synchronous Motor Servo System

HAO YUAN<sup>1</sup>, XIMEI ZHAO<sup>1</sup>, AND DONGXUE FU<sup>1</sup>

School of Electrical Engineering, Shenyang University of Technology, Shenyang 110870, China

Corresponding author: Ximei Zhao (zhaoxm\_sut@163.com)

This article was supported by the Liaoning Provincial Natural Science Foundation of China under Grant 20170540677.

**ABSTRACT** In this paper, an intelligent adaptive jerk control (IAJC) with dynamic compensation gain for the permanent magnet linear synchronous motor (PMLSM) servo system was proposed to improve robustness and tracking performance against nonlinear and time-varying uncertainties. First, the dynamic model of the PMLSM servo system was investigated. Subsequently, the model-based feedforward control was designed for parametric uncertainties. Then, an adaptive jerk control (AJC) was adopted to restrain external load disturbance, nonlinear friction and unmodeled dynamics of the servo system. The adaptive feedback gain of jerk was updated by an exponential function. However, the uncertainties of the PMLSM servo system were unavailable in advance, it was difficult to design the adaptive feedback gain in practice. Thus, in the following part, the IAJC was further developed in which a dynamic compensation gain was designed using a double-loop recurrent feature selection fuzzy neural network (RFSFNN) to compensate for approximation deviation and suppress the chattering phenomenon. The learning algorithms of the double-loop RFSFNN were derived and the stability of the closed-loop system was proved by the Lyapunov approach. Finally, the experimental results demonstrate that the proposed IAC scheme can achieve robust precise tracking performance.

**INDEX TERMS** Intelligent adaptive jerk control, permanent magnet linear synchronous motor, fuzzy neural network, chattering, robustness.

## I. INTRODUCTION

The direct-drive systems have been adopted in many high-performance applications, examples like industrial robots, XY driving devices, CNC machine tools, and two-dimensional micro/nano manufacturing, by virtue of its directly transfer electrical power to mechanical force [1]–[3]. Among these applications, the permanent magnet linear synchronous motor (PMLSM) can achieve higher efficiency, lower thermal losses, better positioning accuracy, and quicker response because the mechanical reduction and transmission parts do not need. Moreover, the nonlinear control performance of the PMLSM servo system can be improved by the vector control theory. Thus, the PMLSM becomes a viable alternative to replace the rotary actuator. However, with the lack of transmission parts, external load

disturbance, nonlinear friction, parametric uncertainties, and unmodeled dynamics in the PMLSM servo system gradually become the main obstacles in the design of the control system [4]. Additionally, the high-performance application of the PMLSM is confined by the nonlinear and time-varying control characteristics. Therefore, it is imperative to adopt a scheme to meet the requirements in the PMLSM servo system.

In the past decade, plenty of compensation methods and observation methods for the linear motor were presented in the literatures. In [5] and [6], the LuGre model and the DNLRX model were presented to cope with the friction force, respectively. In addition, an adaptive observer attenuated periodic disturbances for each repetitive period in [7]. Moreover, dual-relay feedback approaches were obtained to compensate for the friction force model in [8] and [9]. An online tuning adaptive speed and position controllers were developed to achieve the performance in control

The associate editor coordinating the review of this manuscript and approving it for publication was Jinquan Xu<sup>1</sup>.

applications in [10]. However, it is only true when the precise dynamic models of the PMLSM were obtained in these developments.

Typically, sliding mode control (SMC) is a powerful tool which provides enough robustness in different applications mitigates the effect of certain disturbances and system uncertainties when the trajectory reaches and switches on the sliding surface [11], [12]. But the control method often leads to chattering phenomenon caused by the signum function and large switching control gain, which excites high-frequency mode. In addition, the chattering phenomenon makes the control efforts switch back and forth, which may waste energy and damage the servo system. To overcome this problem, researchers look beyond the traditional SMC for some advanced versions. In [13], [14], saturation function, instead of signum function, was in the part of switching laws. Complementary sliding mode control (CSMC) was provided with favorable tracking accuracy in [15], [16]. Moreover, a discrete SMC combined with an incremental PID control was designed for high-speed micro manipulation in [17]. The fractional-order strategy was employed in the SMC system to improve the control performances in [18]. However, the above methods cannot change the structure of SMC, which is a discontinuous control in essence. Therefore, it is important to develop a continuous control scheme that balances the relationship between robustness and chattering.

Recently, a developed control scheme referred as robust integral of the sign of the error (RISE), utilized the integral of the signum term to the jerk of the control as opposed to control signal used in sliding mode directly, was proposed in [19]–[21]. RISE feedback control is originated from super twisting sliding mode control. As long as the matched additive disturbance is smooth enough with known bounds of its time derivatives, the RISE feedback control can achieve asymptotic tracking performance [22]–[25]. More importantly, the resulting control effort is always keeping continuous. In industrial applications, jerk reflects the change in acceleration. In order to achieve high-speed machining, it is required to increase the feed rate in the presence of uncertainties. Recent studies have focused on developments in the feedback gain of the jerk [26]–[28]. In [26], the feedback gain was chosen as a constant. The large-gain feedback could improve the convergence rate, however, it also caused the chattering phenomenon. In [27], an adaptive robust gain was designed to handle the uncertainties, but the results showed that the efficiencies were unfavorable due to the single adaptive law. In [28], the feedback gain was estimated by the multiple adaptive laws, but the approximation deviation due to the system uncertainties remains unavoidably, which the system cannot bear. In order to design a judicious feedback gain, a compensator should be developed to handle the approximation deviation.

A fuzzy neural network (FNN), which combined fuzzy mechanism with neural network, has been successfully employed as a universal compensator in intelligent control technique. FNN can learn from the process with the capability

for identification and present high accuracy to deal with the nonlinearities and uncertainties [29]–[31]. In [32], the structures of the recurrent fuzzy neural network (RFNN) retained superior dynamic ability than simple type. However, the issues of the huge computational burden of the RFNN system have been highly concerned [33], [34]. Besides, it is well known that all features that characterize a data point may not usually be equally important when FNN approximates any continuous function [35], [36]. Hence, to alleviate the computational complexity, it is essential to select favorable feature for the simplicity, identification, and efficiency of the FNN.

The motivation of this paper is to design an intelligent adaptive jerk control scheme (IAJC) for the PMLSM servo system with robustness and high-precision accuracy. The unknown parameters are estimated via the model-based feed-forward and the unmodeled disturbances are compensated via RISE feedback with the jerk adaptation, meanwhile ensuring the continuity of the control effort. The main contributions of this paper are listed as follows:

- 1) A novel exponential adaptive law is designed to the adaptive feedback gain, which effectively reduce the large-gain feedback and control chattering problem of the jerk control. The convergence speed of the exponential adaptive law satisfies the fast convergence requirement.
- 2) Since it is difficult to determine the approximated error of the adaptive feedback gain in real applications. In this paper, a dynamic compensation gain is improved via a double-loop recurrent feature selection fuzzy neural network (RFSFNN).
- 3) The recurrent feature selection neurons are added in the membership layer and the double feedback loop structure is developed for the neural network.

## II. MODELING FOR PMLSM

### A. DYNAMICS OF PMLSM

The mathematical modeling of the PMLSM, which is described in the synchronously rotating reference frame, can be found in [16] and [29]. The electromagnetic thrust dynamic of the PMLSM is expressed as

$$F_e = \frac{3}{2} \cdot \frac{P_n}{2} \cdot \frac{\pi}{\tau} \left[ \psi_f i_q^* + (L_d - L_q) i_d^* i_q^* \right] \quad (1)$$

where  $F_e$  is the electromagnetic thrust;  $P_n$  is the number of pole pairs;  $\tau$  is the pole pitch;  $\psi_f$  is the permanent magnet flux linkage;  $L_d$  and  $L_q$  are the  $d$ - $q$  axis stator inductances;  $i_d^*$  is the flux current command and  $i_q^*$  is the thrust current command. Then, setting  $i_d^*$  as zero for the field-oriented control, the electromagnetic force can be simplified as follows [32]

$$F_e = K_f i_q^* \quad (2)$$

$$K_f = \frac{3}{2} \cdot P_n \cdot \frac{\pi}{\tau} \cdot \psi_f \quad (3)$$

where  $K_f$  is the thrust coefficient.

The dynamic equation of the mover motion with disturbance can be expressed by

$$(M + \Delta M) \ddot{x} + (B + \Delta B) \dot{x} = F_e - F \quad (4)$$

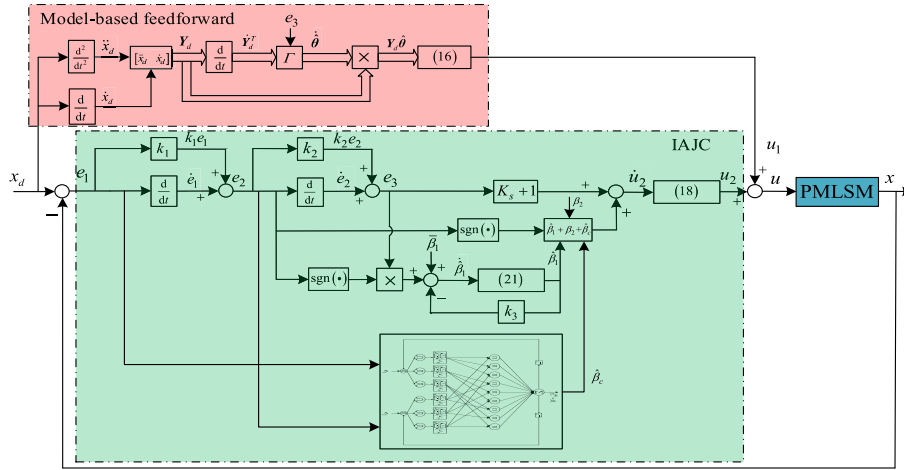


FIGURE 1. Block diagram of the proposed control scheme for PMLSM servo system.

where  $\ddot{x}$  is the acceleration and  $\dot{x}$  is the velocity respectively.  $M$  is the total mass of the mover and  $B$  is the viscous friction coefficient.  $\Delta M$  and  $\Delta B$  are the uncertainties due to mechanical parameters  $M$  and  $B$ .  $F$  is the disturbance including external load disturbance, friction, unmodeled dynamics, etc.

From (2) and (4), the mechanical dynamics of PMLSM can be simplified as

$$\theta_1 \ddot{x} = u - \theta_2 \dot{x} - d \tag{5}$$

where  $\theta_1 = (M + \Delta M)/K_f$ ,  $\theta_2 = (B + \Delta B)/K_f$ ,  $d = F/K_f$ , and  $u = i_q^*$ .  $\theta_1$ ,  $\theta_2$  and  $d$  are time-varying real functions.

**B. PROBLEM FORMULATION FOR PMLSM SERVO SYSTEM**

Although some advantages are mentioned, the control task with challenges is presented. Uncertainties such as nonlinear friction model and parametric uncertainties are difficult to be accurately established. Therefore, a robust control scheme is required to cater to the uncertainties of this model. As a traditional robust control, SMC, which is insensitive to the parametric uncertainties, has been proven to satisfy performance for the system. The control law of SMC contains a signum function to indicate the switching process, so SMC is a discontinuous control. If the initial condition of the nonlinear system is near the original point, it will cause high-frequency oscillation. The high frequency may excite nonlinear dynamics introduced by the uncertainties, which may consume energy and lead to instability. Hence, it is necessary to design a control scheme to ensure the robustness of the system and accuracy of feedback control in the presence of model uncertainties, while avoiding the phenomenon of chattering.

**III. PROPOSED CONTROL SYSTEMS**

To ensure minimal excitation of nonlinear dynamics, the control input signal should be smooth and continuous. Therefore, it is important not only to focus on the control law  $u$  but also to design the derivative of the control law, that is, the jerk signal. However, due to the model uncertainties, fast response to the tracking error may still require a high jerk control signal.

To satisfy stability and rapidity, a RISE feedback control scheme is proposed on the basis of the intelligent adaptive jerk and model-based feedforward. The block diagram of the proposed control scheme for the PMLSM servo system is shown in Fig. 1.

**A. CONSTRUCTION OF CONTROL SYSTEM**

Due to the existence of nonlinear dynamics, it is desirable to find a control law that the mover position  $x$  can track the reference command  $x_d$  while minimizing the chattering of control signals. To quantify the design of the following controllers, the filtered error vector is defined as

$$z = [e_1 \ e_2 \ e_3]^T \tag{6}$$

$$\begin{aligned} e_1 &= x_d - x \\ e_2 &= \dot{e}_1 + k_1 e_1 \\ e_3 &= \dot{e}_2 + k_2 e_2 \end{aligned} \tag{7}$$

where  $x_d$  is the reference command;  $e_1$ ,  $e_2$  and  $e_3$  are the position tracking error, filtered velocity error and filtered accelerate error respectively.  $k_1, k_2 \in \mathbb{R}$  denote positive constants control gains. The filtered error  $e_3$  is introduced to facilitate the stability analysis and is not measurable in the controller design since the expression in (7) depends on  $\ddot{x}$ .

The open-loop tracking error system can be developed by the right multiplying (7) by  $\theta_1$  and utilizing the expressions in (5) to obtain the following expression

$$\begin{aligned} \theta_1 e_3 &= \theta_1 (\ddot{x}_d - \ddot{x}) + \theta_1 (k_1 \dot{e}_1 + k_2 e_2) \\ &= \theta_1 \ddot{x}_d - (u - \theta_2 \dot{x} - d) + \theta_1 (k_1 \dot{e}_1 + k_2 e_2) \\ &= \theta_1 \ddot{x}_d - u + \theta_2 \dot{x} + d + \theta_1 (k_1 \dot{e}_1 + k_2 e_2) + \theta_2 \dot{x}_d - \theta_2 \dot{x}_d \\ &= \theta_1 \ddot{x}_d + \theta_2 \dot{x}_d + \theta_1 (k_1 \dot{e}_1 + k_2 e_2) - \theta_2 \dot{e}_1 + d - u \\ &= Y_d \theta + S + d - u \end{aligned} \tag{8}$$

where  $Y_d = [\ddot{x}_d, \dot{x}_d]$  refers to the reference command vector and  $\theta = [\theta_1 \ \theta_2]^T$  is the parameter vector.  $S$  is defined to be

$$S = \theta_1 (k_1 \dot{e}_1 + k_2 e_2) - \theta_2 \dot{e}_1 \tag{9}$$

Different from the conventional robust control, the filtered error will introduce into the availability of additional

design freedom. Therefore, the two-degrees-of-freedom control structure is adopted. The control law is structured (8) as

$$u = u_1 + u_2 \quad (10)$$

Here,  $u_1$  is the feedforward term to speed up the response and cater for parametric uncertainty, expressed as

$$u_1 = Y_d \hat{\theta} \quad (11)$$

where  $\hat{\theta}$  denotes the estimate of  $\theta$  and  $u_2$  is the feedback control law to ensure the robustness of the closed-loop system when the system is suffered from external disturbances and unmodeled uncertainties. Since the reference command vector  $Y_d$  and its time derivative depend on the reference command only, they can be calculated offline so that the online computation time will be saved and the measurement noise is reduced. Thus, it is more suitable for practical applications.

To avoid the excitation of the resonant modes, it is important to ensure that the control signal  $u_2$  is continuous, the jerk signal  $\dot{u}_2$  should be bounded. Hence, the time derivative is taken on the closed-loop tracking error system of (8)

$$\theta_1 \dot{e}_3 = -\frac{1}{2} \dot{\theta}_1 e_3 + \dot{Y}_d \tilde{\theta} + \tilde{N} + N_d - \dot{u}_2 - e_2 \quad (12)$$

where  $\tilde{\theta} = \theta - \hat{\theta}$  refers to the parameter estimation error vector and the unmeasurable terms  $\tilde{N}$  and  $N_d$  are defined to be

$$\tilde{N}(t) = Y_d \dot{\tilde{\theta}} + \dot{S} + e_2 - \frac{1}{2} \dot{\theta}_1 e_3 \quad (13)$$

$$N_d(t) = \dot{d} \quad (14)$$

It is a fact that the  $\tilde{N}$  and  $N_d$  in (13) and (14) have different bounds, which facilitates the development of the  $\hat{\theta}$  update law and the subsequent stability analysis. Here,  $\hat{\theta}$  is designed based on a gradient-based adaptive update law, as in [27], and is given by

$$\dot{\hat{\theta}} = \Gamma \dot{Y}_d^T e_3 \quad (15)$$

where  $\Gamma \in \mathbb{R}$  is a positive scalar gain. To avoid utilizing  $\ddot{x}$  for calculating  $e_3$ , the feedforward control law  $u_1$  is integrated by parts as

$$Y_d \hat{\theta} = Y_d \hat{\theta}(0) + Y_d \Gamma \dot{Y}_d^T e_2(\tau) \Big|_0^t - Y_d \Gamma \int_0^t \left[ \ddot{Y}_d^T e_2(\tau) - k_2 \dot{Y}_d^T e_2(\tau) \right] d\tau \quad (16)$$

where  $\hat{\theta}(0)$  is the value of  $\hat{\theta}(t)$  when  $t = 0$ .

### B. INTELLIGENT ADAPTIVE JERK CONTROL

The jerk  $\dot{u}_2$  of the RISE feedback control term is designed to be

$$\dot{u}_2 = (K_s + 1) e_3 + (\hat{\beta}_1 + \beta_2 + \hat{\beta}_c) \text{sgn}(e_2) \quad (17)$$

where  $\hat{\beta}_1 > -\beta_2$  and  $\beta_2 > 0$  are adaptive feedback gain and fixed feedback gain according to the jerk respectively,  $\hat{\beta}_c$  is the dynamic compensation gain which is designed by a dynamic neural network to refine the adaptive feedback

gain  $\hat{\beta}_1$ . Accordingly, the feedback control law  $u_2$  with the integral term is given by

$$\begin{aligned} u_2(t) &= (K_s + 1) \int_0^t (\dot{e}_2(\tau) + k_2(\dot{e}_1(\tau) + k_1 e_1(\tau))) d\tau \\ &\quad + \int_0^t (\hat{\beta}_1 + \beta_2 + \hat{\beta}_c) \text{sgn}(e_2(\tau)) d\tau + u_2(0) \\ &= (K_s + 1) [(e_2(t) - e_2(0)) + k_2(e_1(t) - e_1(0)) \\ &\quad + k_1 k_2 \int_0^t e_1(\tau) d\tau] + \int_0^t (\hat{\beta}_1 + \beta_2 + \hat{\beta}_c) \\ &\quad \times \text{sgn}(e_2(\tau)) d\tau + u_2(0) \\ &= (K_s + 1) \left[ \dot{e}_1 + (k_1 + k_2) e_1 + k_1 k_2 \int_0^t e_1(\tau) d\tau \right] \\ &\quad + \int_0^t (\hat{\beta}_1 + \beta_2 + \hat{\beta}_c) \text{sgn}(e_2(\tau)) d\tau + E_0 + u_2(0) \end{aligned} \quad (18)$$

where  $K_s > 0$ ,  $u_2(0)$  is the value of  $u_2(t)$  when  $t = 0$ ,  $E_0$  is the offset due to initial conditions, expressed as

$$E_0 = -(K_s + 1) [k_2 e_1(0) + e_2(0)] \quad (19)$$

Due to the structural complexity of the disturbance, it is very difficult to find its precise limits, even in practice. If boundaries are sometimes available, they are usually very conservative. Large-gain feedback will result in serious design conservativeness, while too small selection may result in performance degradation or even instability, such as high-frequency resonance. To avoid the negative effect of excessive feedback gain,  $\hat{\beta}_1$  is proposed as

$$\dot{\hat{\beta}}_1 = -k_3 \hat{\beta}_1 + \bar{\beta}_1 + e_3 \text{sgn}(e_2) \quad (20)$$

where  $\bar{\beta}_1, k_3$  are constants. Let  $\hat{\beta}_1$  converge exponentially to  $\beta_1 = \bar{\beta}_1/k_3$ , then  $\hat{\beta}_1$  yields

$$\begin{aligned} \hat{\beta}_1 &= \beta_1 \left( 1 - e_2^{-k_3 t} \right) + |e_2| - e_2^{-k_3 t} |e_2(0)| \\ &\quad + e_2^{-k_3 t} \hat{\beta}_1(0) + (k_2 - k_3) e_2^{-k_3 t} * |e_2(t)| \end{aligned} \quad (21)$$

where  $(*)$  denotes the convolution operator. Compared with the jerk law with the fixed RISE feedback gain,  $u$  will respond faster to adjust the filtered error back to zero.

### C. DOUBLE-LOOP RECURRENT FEATURE SELECTION FUZZY NEURAL NETWORK

In order to increase the approximating capacity of the adaptive feedback gain, and to improve the robustness and dynamic tracking accuracy of the PMLSM servo system, accordingly, the proposed double-loop RFSFNN combines the features of FNN, recurrent structure, and feature selection. The proposed double-loop RFSFNN is a new structure of recurrent feature selection fuzzy neural network with a double feedback loop, where the recurrent weight and the output signal in the previous step are memorized and utilized as the feedback signal in the internal loop and external loop. The merit of the structure is that the internal state information and output signal are captured at the same time, thus, it can achieve better approximation performance compared with the single-loop RFNN. In addition, the feature selection layer,

which is incorporated by the recurrent feature selection and Gaussian membership functions, and the rule layer are the hidden layers. In other words, the appearance of the recurrent feature selection will make double-loop RFSFNN become a dynamic structure that has enough ability to deal with uncertainties of the PMLSM servo system.

1) LAYER 1—INPUT LAYER

The nodes in layer 1 transmit the input signals to the next layer. The input variables are the filtered error  $e_1, e_2$ . For every node  $i$  in this layer, the input and the output of the double-loop RFSFNN can be represented as

$$net_i^{(1)}(N) = \prod_o x_i^{(1)}(N) y_o^{(4)}(N-1), \quad o = 1 \tag{22}$$

$$y_i^{(1)}(N) = f_i^{(1)}(net_i^{(1)}(N)) = net_i^{(1)}(N), \quad i = 1, 2 \tag{23}$$

where  $x_i^{(1)}(N)$  represents the input of  $i$ th node in this layer,  $x_1^{(1)} = e_1, x_2^{(1)} = e_2$ ;  $net_i^{(1)}(N)$  represents inputs of the network where the superscript is the layer number and subscript is the node number;  $y_o^{(4)}$  is the output of double-loop RFSFNN and  $y_i^{(1)}(N)$  is the output of  $i$ th node;  $N$  is the number of the sampling iteration;  $f_i^{(1)}$  is a unit function of the  $i$ th node.

2) LAYER 2—FEATURE SELECTION LAYER

In this layer, each output from layer 1 is connected to three neurons that act as a linguistic label of one of the input variables. Moreover, Gaussian function is adopted as the membership function, and feature selection with a unit of memory is determined in this layer. For the  $j$  node, the relationship of the input and output can be described as

$$net_j^{(2)}(N) = \left[ -\frac{(x_i^{(2)}(N) - m_{ij})^2}{(\sigma_{ij})^2} \right] \tag{24}$$

$$y_j^{(2)}(N) = f_j^{(2)}(net_j^{(2)}(N)) \alpha_j(N) = \left[ \exp(net_j^{(2)}(N)) \right] \cdot \left[ 1 - \exp(-(\delta_j(N) w_j \delta_j(N-1))^2) \right], \quad j = 1, \dots, 6 \tag{25}$$

$$d_{jk}(N) = \begin{cases} M, & \alpha_j(N) \leq T_j \\ 1, & \text{otherwise} \end{cases} \tag{26}$$

where  $x_i^{(2)}(N) = y_i^{(1)}(N)$  is the input of this layer;  $m_{ij}$  and  $\sigma_{ij}$  are the mean and standard deviation, respectively, of the Gaussian functions of the  $j$ th term associated with the  $i$ th input variable.  $f_j^{(2)}$  is an exponential function of the  $j$ th node;  $f_j^{(2)}(net_j^{(2)}(N))$  is the Gaussian function output;  $\alpha_j(N) = \left[ 1 - \exp(-(\delta_j(N) w_j \delta_j(N-1))^2) \right]$  is the door adjuster that can adjust the door, which state is opened or closed.  $\delta_j(N)$  is the feature degree parameter of the  $j$ th node;  $w_j$  is the recurrent weight of  $j$ th node;  $T_j$  is a threshold value, expressed as

$$T_j = \frac{1}{1 + \kappa (e_1^2 + e_2^2)} \tag{27}$$

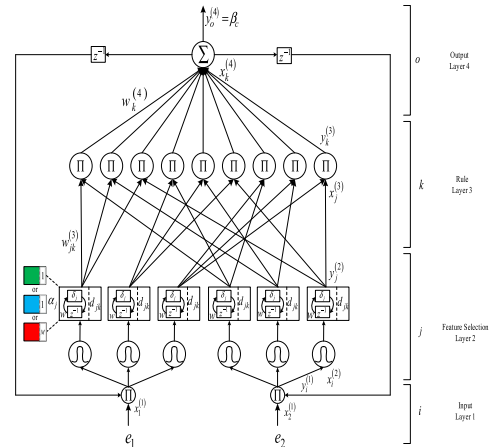


FIGURE 2. Structure of the double-loop RFSFNN.

TABLE 1. Relationships between data, Features, Door statuses, Doorplate, and door adjuster.

$j$	Data	Features	Door statuses	Doorplate $d_{jk}(N)$	Door adjuster $\alpha_j(N)$
	Most useful	Full select	Full open	1	1
	Useful	Partially select	Partially open	1	$(T_j 1)$
	Unfavourable	Discard	Close	$M$	$(0 T_j)$

where  $\kappa$  is a positive gain. It is worth noticing that the values of  $T_j$  are related to the tracking error. If the tracking error becomes larger, the values of  $T_j$  will be decreased and there are more control rules transmitted in the neural network. Contrarily, if the tracking error becomes smaller, the values of  $T_j$  will be raised and the control rules will be reduced. According to this mechanism, the adaptability of the fuzzy operator can be enhanced, and the unfavorable features are eliminated;  $M$  is the door mark, which is a positive constant and bigger than 1, and  $M$  is set to be 2 in this study;  $d_{jk}(N)$  is the doorplate of the  $j$ th term associated with  $k$ th term node. If  $\alpha_j(N)$  is equal to 1, the output of Gaussian function will be the most useful data in the system and the door will fully open. If the value of  $\alpha_j(N)$  is between 1 and 0, the output of Gaussian function will be the useful data in the system and the door will partially open. If  $\alpha_j(N)$  is equal to  $T_j$  or smaller than  $T_j$ , the output of Gaussian function will be the unfavorable data in the system and the door will close. The relationships between data, features, door statuses, doorplate, and door adjuster are shown in Table 1.

3) LAYER 3—RULE LAYER

Each node  $k$  in this layer represents one feature selection rule and performs precondition matching of a rule. Hence, the neuron in this layer is denoted by  $\Pi$ , which multiplies the input signals from layer 2 and outputs the result of

the product. For every  $k$ th node

$$\begin{aligned} net_k^{(3)}(N) &= \prod_j w_{jk}^{(3)} x_j^{(3)}(N) \end{aligned} \quad (28)$$

$$y_k^{(3)}(N) = \begin{cases} \max(w_{jk}^{(3)} x_j^{(3)}(N), w_{jk}^{(3)} x_j^{(3)}(N)), \\ d_{jk}(N) d_{jk}(N) = M \\ f_k^{(3)}(net_k^{(3)}) = net_k^{(3)}, \text{ otherwise} \end{cases} \quad (29)$$

$k = 1, \dots, 9$

where  $x_j^{(3)}(N) = y_j^{(2)}(N)$  is the input in this layer;  $w_{jk}^{(3)}$ , which is set to 1 simplify the implementation for the real-time control, is the connected weight between the feature selection layer and the rule layer;  $y_k^{(3)}(N)$  is the output in this layer;  $f_k^{(3)}$  is a unity function of the  $k$ th node. In (29), if  $d_{jk}(N) d_{jk}(N) = M$ , there are two possible conditions for the status of the door adjuster: 1) full open and close and 2) partially open and close. On the other hand,  $d_{jk}(N) d_{jk}(N) \neq M$ , there are four possible conditions for the status of the door adjuster: 1) both full open; 2) both partially open; 3) one fully open and one partially open; and 4) both close.

#### 4) LAYER 4—OUTPUT LAYER

The single in this layer is denoted by  $\Sigma$ , which computes the overall output as the summation of all input. the output node together with related links acts as a defuzzifier. The mathematical function can be stated as

$$net_o^{(4)}(N) = \sum_k w_k^{(4)} x_k^{(4)}(N) \quad (30)$$

$$y_o^{(4)}(N) = f_o^{(4)}(net_o^{(4)}) = net_o^{(4)} \quad (31)$$

where  $x_k^{(4)}$  is the output of rule layer;  $w_k^{(4)}$  is the connected weight between the rule layer and the output layer;  $y_o^{(4)}$  is the final output of double-loop RFSFNN and also estimated nonlinear function  $\beta_c$ .

#### D. LEARNING ALGORITHMS OF THE DOUBLE-LOOP RFSFNN

The final output of double-loop RFSFNN can be rewritten as

$$\beta_c(e_1, e_2, \mathbf{W}, \mathbf{m}, \boldsymbol{\sigma}, \mathbf{R}, \boldsymbol{\delta}) \equiv \mathbf{W}\mathbf{X} \quad (32)$$

where  $\mathbf{W} = [w_1^{(4)} w_2^{(4)} w_3^{(4)} w_4^{(4)} w_5^{(4)} w_6^{(4)} w_7^{(4)} w_8^{(4)} w_9^{(4)}] \in \mathbb{R}^{1 \times 9}$  is a vector matrix formed by weight  $w_k^{(4)}$ , which is updated by the online learning algorithm and initialized to be zero;  $\mathbf{X} = [x_1^{(4)} x_2^{(4)} x_3^{(4)} x_4^{(4)} x_5^{(4)} x_6^{(4)} x_7^{(4)} x_8^{(4)} x_9^{(4)}]^T \in \mathbb{R}^{9 \times 1}$  is the output vector matrix;  $\mathbf{m} = [m_{11} m_{12} \dots m_{25} m_{26}]^T \in \mathbb{R}^{6 \times 1}$  and  $\boldsymbol{\sigma} = [\sigma_{11} \sigma_{12} \dots \sigma_{25} \sigma_{26}]^T \in \mathbb{R}^{6 \times 1}$  are the mean vector matrix and standard deviation vector matrix, respectively;  $\mathbf{R} = [w_1 w_2 \dots w_5 w_6] \in \mathbb{R}^{6 \times 1}$  is the recurrent weight vector matrix;  $\boldsymbol{\delta} = [\delta_1 \delta_2 \dots \delta_5 \delta_6]^T \in \mathbb{R}^{6 \times 1}$  is the feature degree parameter vector matrix.

By the universal approximation theorem, there exists an optimal double-loop RFSFNN  $\beta_c^*$  for any nonlinear function such that

$$\begin{aligned} \beta_c &= \beta_c^*(e_1, e_2, \mathbf{W}^*, \mathbf{m}^*, \boldsymbol{\sigma}^*, \mathbf{R}^*, \boldsymbol{\delta}^*) + \varepsilon \\ &= \mathbf{W}^* \mathbf{X}^* + \varepsilon \end{aligned} \quad (33)$$

where  $\varepsilon$  is a minimum reconstructed error;  $\mathbf{W}^*, \mathbf{m}^*, \boldsymbol{\sigma}^*, \mathbf{R}^*, \boldsymbol{\delta}^*$  and  $\mathbf{X}^*$  are the optimal parameters of  $\mathbf{W}, \mathbf{m}, \boldsymbol{\sigma}, \mathbf{R}, \boldsymbol{\delta}$  and  $\mathbf{X}$ , respectively. Moreover, the four-layer double-loop RFSFNN approximation for  $\beta_c$  is given as

$$\hat{\beta}_c(e_1, e_2, \hat{\mathbf{W}}, \hat{\mathbf{m}}, \hat{\boldsymbol{\sigma}}, \hat{\mathbf{R}}, \hat{\boldsymbol{\delta}}) := \hat{\mathbf{W}} \hat{\mathbf{X}} \quad (34)$$

where  $\hat{\mathbf{W}}, \hat{\mathbf{m}}, \hat{\boldsymbol{\sigma}}, \hat{\mathbf{R}}, \hat{\boldsymbol{\delta}}$  and  $\hat{\mathbf{X}}$  are the estimated parameters of  $\mathbf{W}, \mathbf{m}, \boldsymbol{\sigma}, \mathbf{R}, \boldsymbol{\delta}$  and  $\mathbf{X}$ , respectively. Subtracting (34) from (33), the approximation error  $\tilde{\beta}_c$  can be obtained

$$\begin{aligned} \tilde{\beta}_c &= \beta_c^*(e_1, e_2, \mathbf{W}^*, \mathbf{m}^*, \boldsymbol{\sigma}^*, \mathbf{R}^*, \boldsymbol{\delta}^*) + \varepsilon \\ &\quad - \hat{\beta}_c(e_1, e_2, \hat{\mathbf{W}}, \hat{\mathbf{m}}, \hat{\boldsymbol{\sigma}}, \hat{\mathbf{R}}, \hat{\boldsymbol{\delta}}) \\ &= \mathbf{W}^* \mathbf{X}^* + \varepsilon - \hat{\mathbf{W}} \hat{\mathbf{X}} \\ &= \tilde{\mathbf{W}} \mathbf{X}^* + \hat{\mathbf{W}} \tilde{\mathbf{X}} + \varepsilon \end{aligned} \quad (35)$$

where  $\tilde{\mathbf{W}} = \mathbf{W}^* - \hat{\mathbf{W}}$  and  $\tilde{\mathbf{X}} = \mathbf{X}^* - \hat{\mathbf{X}}$ . Then, the linearization technique is used to transform the nonlinear output of the double-loop RFSFNN into partially linear form to obtain the expansion of  $\tilde{\mathbf{X}}$  in Taylor series is obtained as

$$\tilde{\mathbf{X}} = \mathbf{X}_m^T \tilde{\mathbf{m}} + \mathbf{X}_\sigma^T \tilde{\boldsymbol{\sigma}} + \mathbf{X}_R^T \tilde{\mathbf{R}} + \mathbf{X}_\delta^T \tilde{\boldsymbol{\delta}} + N_h \quad (36)$$

where  $\tilde{\mathbf{m}} = \mathbf{m}^* - \hat{\mathbf{m}}; \tilde{\boldsymbol{\sigma}} = \boldsymbol{\sigma}^* - \hat{\boldsymbol{\sigma}}; \tilde{\mathbf{R}} = \mathbf{R}^* - \hat{\mathbf{R}}; \tilde{\boldsymbol{\delta}} = \boldsymbol{\delta}^* - \hat{\boldsymbol{\delta}};$  and  $N_h$  is a vector of higher order terms;

$$\begin{aligned} \mathbf{X}_m^T &= \left[ \begin{array}{ccc} \frac{\partial x_1^{(4)}}{\partial m_{11}} & \dots & \frac{\partial x_1^{(4)}}{\partial m_{26}} \\ \vdots & \ddots & \vdots \\ \frac{\partial x_9^{(4)}}{\partial m_{11}} & \dots & \frac{\partial x_9^{(4)}}{\partial m_{26}} \end{array} \right]_{m_{ij}=\hat{m}_{ij}} \in \mathbb{R}^{9 \times 6} \\ \mathbf{X}_\sigma^T &= \left[ \begin{array}{ccc} \frac{\partial x_1^{(4)}}{\partial \sigma_{11}} & \dots & \frac{\partial x_1^{(4)}}{\partial \sigma_{26}} \\ \vdots & \ddots & \vdots \\ \frac{\partial x_9^{(4)}}{\partial \sigma_{11}} & \dots & \frac{\partial x_9^{(4)}}{\partial \sigma_{26}} \end{array} \right]_{\sigma_{ij}=\hat{\sigma}_{ij}} \in \mathbb{R}^{9 \times 6} \\ \mathbf{X}_R^T &= \left[ \begin{array}{ccc} \frac{\partial x_1^{(4)}}{\partial w_1} & \dots & \frac{\partial x_1^{(4)}}{\partial w_6} \\ \vdots & \ddots & \vdots \\ \frac{\partial x_9^{(4)}}{\partial w_1} & \dots & \frac{\partial x_9^{(4)}}{\partial w_6} \end{array} \right]_{w_j=\hat{w}_j} \in \mathbb{R}^{9 \times 6} \\ \mathbf{X}_\delta^T &= \left[ \begin{array}{ccc} \frac{\partial x_1^{(4)}}{\partial \delta_1} & \dots & \frac{\partial x_1^{(4)}}{\partial \delta_6} \\ \vdots & \ddots & \vdots \\ \frac{\partial x_9^{(4)}}{\partial \delta_1} & \dots & \frac{\partial x_9^{(4)}}{\partial \delta_6} \end{array} \right]_{\delta_j=\hat{\delta}_j} \in \mathbb{R}^{9 \times 6} \end{aligned}$$

The adaptation laws of the double-loop RFSFNN are designed as

$$\dot{\tilde{W}}^T = -\eta_w e_2 \hat{X}^T \quad (37)$$

$$\dot{\tilde{m}}^T = -\eta_m e_2 \hat{W} X_m^T \quad (38)$$

$$\dot{\tilde{\sigma}}^T = -\eta_\sigma e_2 \hat{W} X_\sigma^T \quad (39)$$

$$\dot{\tilde{R}}^T = -\eta_R e_2 \hat{W} X_R^T \quad (40)$$

$$\dot{\tilde{\delta}}^T = -\eta_\delta e_2 \hat{W} X_\delta^T \quad (41)$$

where  $\eta_w, \eta_m, \eta_\sigma, \eta_R$  and  $\eta_\delta$  are learning rates parameters and all set as positive constants.

### E. STABILITY ANALYSIS OF THE INTELLIGENT ADAPTIVE JERK CONTROL SYSTEM

*Assumption 1:* Uncertainty  $d$  is smooth enough such that [37]

$$\|N_d(t)\|_1 \leq \varsigma_1, \|\dot{N}_d(t)\|_1 \leq \varsigma_2 \quad (42)$$

where  $\varsigma_1 > 0, \varsigma_2 > 0$  are known constants.

Since  $\tilde{N}$  is continuous, by the Mean Value Theorem, its norm can be upper bounded by a positive, non-decreasing function  $\rho$  as

$$\|\tilde{N}\| \leq \rho(\|z\|) \|z\| \quad (43)$$

*Theorem 1:* Consider the system (8) controlled by the two-degrees-of-freedom control structure (10), with feedforward (16) and feedback (18) including adaptive feedback gain (21) and the dynamic adaptation (34). If the model mismatch (13) and the disturbance (14) are bounded by (42) and (43) accordingly, and  $K_s$  is selected such that

$$K_s > \frac{\rho^2(\|z\|)}{4\eta_3} \quad (44)$$

where  $\eta_3 = \min\{k_1 - \frac{1}{2}, k_2 - \frac{1}{2}, 1\}, k_1 > \frac{1}{2}$  and  $k_2 > \frac{1}{2}$ .  $\square$

For  $\beta_1 \geq \varsigma_1 + \frac{1}{k_2} \varsigma_2$  and  $\beta_2 \geq 0$ , auxiliary functions  $L_1, L_2$  are defined as

$$L_1 = e_3 (N_d(t) - \beta_1 \text{sgn}(e_2)) \quad (45)$$

$$L_2 = -\beta_2 \dot{e}_2 \text{sgn}(e_2) \quad (46)$$

Provided the sufficient conditions  $\beta_1$  and  $\beta_2$  are satisfied, the following inequality can be obtained [26], [28]

$$\int_0^t L_1(\tau) d\tau \leq \varsigma_{b1} \quad (47)$$

$$\int_0^t L_2(\tau) d\tau \leq \varsigma_{b2} \quad (48)$$

where  $\varsigma_{b1}, \varsigma_{b2}$  are positive constants. Then, the following defined function  $P_1, P_2$  are always positive

$$P_1 = \varsigma_{b1} - \int_0^t L_1(\tau) d\tau \geq 0 \quad (49)$$

$$P_2 = \varsigma_{b2} - \int_0^t L_2(\tau) d\tau \geq 0 \quad (50)$$

$y(t)$  is defined as

$$y(t) = \left[ z^T(t) \tilde{\theta}^T(t) \tilde{\beta}_1(t) \tilde{\beta}_c(t) \sqrt{P_1} \sqrt{P_2} \right]^T \quad (51)$$

Considering the Lyapunov function  $V(y, t)$  be defined as

$$V(y, t) = \frac{1}{2} e_1^2 + \frac{1}{2} e_2^2 + \frac{1}{2} e_3^2 \theta_1 + \frac{1}{2} \tilde{\theta}^T \Gamma^{-1} \tilde{\theta} + \frac{1}{2} \tilde{\beta}_1^2 + \frac{1}{2} \tilde{\beta}_c^2 + P_1 + P_2 \quad (52)$$

where  $\tilde{\beta}_1 = \beta_1 - \hat{\beta}_1$ . Moreover, the approximated compensate gain  $\beta_c$  is assumed to be bounded by  $|\beta_c| \leq \beta_b, \beta_b$  is a positive gain. Since the sampling interval in the experiment is short enough,  $\beta_c$  is also assumed to be a constant during the approximation. However, the upper bound  $\beta_b$  is difficult to know. Therefore, an adaptive law is proposed to adopt the value of the dynamic approximated compensate for gain. Then, differentiate  $\hat{\beta}_c$  with respect to time, one can obtain  $\dot{\hat{\beta}}_c = -\hat{\beta}_c$ .

$V(y, t) \geq 0$  since  $P_1 \geq 0, P_2 \geq 0$  and other terms are quadratic. In addition,

$$\eta_1 \|y\|^2 \leq V(y, t) \leq \eta_2 \|y\|^2 \quad (53)$$

where  $\eta_1 = \frac{1}{2} \min\{1, m, \Gamma^{-1}\}, \eta_2 = \frac{1}{2} \max\{2, \bar{M}, \Gamma^{-1}\}, m = \inf(\theta_1)$ , and  $\bar{M} = \sup(\theta_1)$ . Then it yields

$$\dot{V}(y, t) = e_1 \dot{e}_1 + e_2 \dot{e}_2 + e_3 \dot{e}_3 \theta_1 + \frac{1}{2} e_3^2 \dot{\theta}_1 + \tilde{\theta}^T \Gamma^{-1} \dot{\tilde{\theta}} + \dot{P}_1 + \dot{P}_2 + \tilde{\beta}_1 \dot{\hat{\beta}}_1 + \tilde{\beta}_c \dot{\hat{\beta}}_c \quad (54)$$

With substituting equations (6), (12), (15), (17), (49), and (50) into equation (54)

$$\begin{aligned} \dot{V} &= e_1 (e_2 - k_1 e_1) + e_2 (e_3 - k_2 e_2) + e_3 \left( -\frac{1}{2} \dot{\theta}_1 e_3 + \dot{Y}_d \tilde{\theta} + \tilde{N} \right. \\ &\quad \left. + N_d - \dot{u}_2 - e_2 \right) + \frac{1}{2} e_3^2 \dot{\theta}_1 + \tilde{\theta}^T \Gamma^{-1} \left( -\Gamma \dot{Y}_d^T e_3 \right) - e_3 (N_d \\ &\quad - \beta_1 \text{sgn}(e_2)) + \beta_2 \dot{e}_2 \text{sgn}(e_2) + \tilde{\beta}_1 \left( \dot{\hat{\beta}}_1 - \dot{\hat{\beta}}_1 \right) - \tilde{\beta}_c \dot{\hat{\beta}}_c \\ &= e_1 e_2 - k_1 e_1^2 + e_2 e_3 - k_2 e_2^2 - \frac{1}{2} \dot{\theta}_1 e_3^2 + e_3 \dot{Y}_d \tilde{\theta} + e_3 \left( \tilde{N} \right. \\ &\quad \left. + N_d - \dot{u}_2 \right) - e_2 e_3 + \frac{1}{2} e_3^2 \dot{\theta}_1 - \tilde{\theta}^T \dot{Y}_d^T e_3 - e_3 (N_d \\ &\quad - \beta_1 \text{sgn}(e_2)) + \beta_2 \dot{e}_2 \text{sgn}(e_2) - \tilde{\beta}_1 \dot{\hat{\beta}}_1 - \tilde{\beta}_c \dot{\hat{\beta}}_c \\ &= e_1 e_2 - k_1 e_1^2 - k_2 e_2^2 + e_3 \left( \tilde{N} + N_d - (K_s + 1) e_3 \right. \\ &\quad \left. - \left( \hat{\beta}_1 + \beta_2 + \hat{\beta}_c \right) \text{sgn}(e_2) \right) - e_3 (N_d - \beta_1 \text{sgn}(e_2)) \\ &\quad + \beta_2 \dot{e}_2 \text{sgn}(e_2) - \tilde{\beta}_1 \dot{\hat{\beta}}_1 - \tilde{\beta}_c \dot{\hat{\beta}}_c \\ &= e_1 e_2 - k_1 e_1^2 - k_2 e_2^2 + e_3 \tilde{N} + e_3 N_d - K_s e_3^2 - e_3^2 \\ &\quad - e_3 \left( \hat{\beta}_1 - \beta_1 \right) \text{sgn}(e_2) + \beta_2 (\dot{e}_2 - e_3) \text{sgn}(e_2) \\ &\quad - e_3 \hat{\beta}_c \text{sgn}(e_2) - e_3 N_d - \tilde{\beta}_1 \dot{\hat{\beta}}_1 - \tilde{\beta}_c \dot{\hat{\beta}}_c \\ &= e_1 e_2 - k_1 e_1^2 - k_2 e_2^2 + e_3 \tilde{N} - K_s e_3^2 - e_3^2 \\ &\quad - e_3 \left( -\tilde{\beta}_1 \right) \text{sgn}(e_2) \\ &\quad - \beta_2 k_2 e_2 \text{sgn}(e_2) - e_3 \hat{\beta}_c \text{sgn}(e_2) - \tilde{\beta}_1 \dot{\hat{\beta}}_1 - \tilde{\beta}_c \dot{\hat{\beta}}_c \end{aligned} \quad (55)$$

According to

$$e_1 e_2 \leq \frac{1}{2} e_1^2 + \frac{1}{2} e_2^2 \quad (56)$$

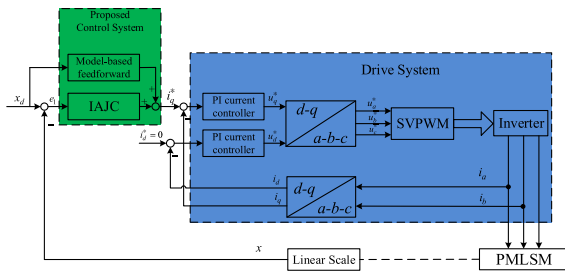
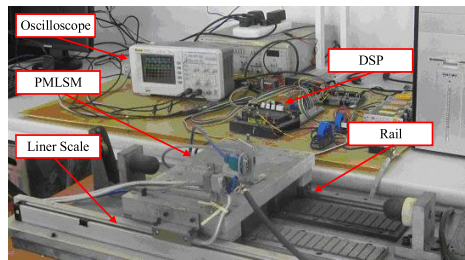
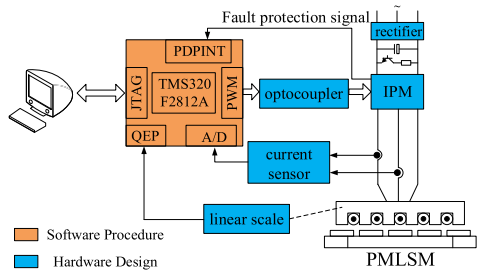


FIGURE 3. Block diagram of the PMLSM drive system using the proposed control system.



(a) Experimental setup



(b) Block diagram of the DSP-based control system

FIGURE 4. DSP-based IAJC for PMLSM servo system.

TABLE 2. Parameters of PMLSM.

Symbol	Value	Unit
$K_f$	50	N/A
$L_d$	41.4	mH
$L_q$	41.4	mH
$\psi_f$	0.09	Wb
$\tau$	32	mm
$M$	16	kg
$B$	8	N-s/m

substituting equation (56) into (55) and combining (43), it yields

$$\begin{aligned}
 \dot{V} &\leq \frac{1}{2}e_1^2 + \frac{1}{2}e_2^2 - k_1e_1^2 - k_2e_2^2 + |e_3| \rho(\|z\|) \|z\| \\
 &\quad - K_s e_3^2 - e_3^2 - |e_3 \tilde{\beta}_1| - |e_3 \tilde{\beta}_c| \\
 &\quad - |\tilde{\beta}_1 \dot{\tilde{\beta}}_1| - |\tilde{\beta}_c \dot{\tilde{\beta}}_c| \\
 &\leq -\left(k_1 - \frac{1}{2}\right) e_1^2 - \left(k_2 - \frac{1}{2}\right) e_2^2 - e_3^2 + \rho(\|z\|) \|z\|^2 - K_s e_3^2 \\
 &\leq -\eta_3 \|z\|^2 + \rho(\|z\|) \|z\|^2 - K_s e_3^2 \\
 &\leq -\|z\|^2 \left(\eta_3 - \frac{\rho^2(\|z\|)}{4K_s}\right) \tag{57}
 \end{aligned}$$

TABLE 3. Parameters of controllers.

	Parameters	Value
IAJC	$K$	2.5
	$\eta_w$	0.1
	$\eta_m$	0.05
	$\eta_\sigma$	0.02
	$\eta_R$	0.001
	$\eta_\delta$	0.002
AJC	$k_1$	2
	$k_2$	70
	$k_3$	6
	$\hat{\beta}_1(0)$	1
	$\tilde{\beta}_1$	30
	$\beta_1$	5
	$\beta_2$	0.5
	$\Gamma$	15
	$K_s$	52
	SMC	$B_n$
$A_n$		-0.62
$\lambda$		60
$\Theta$		9
$\Phi$		0.001

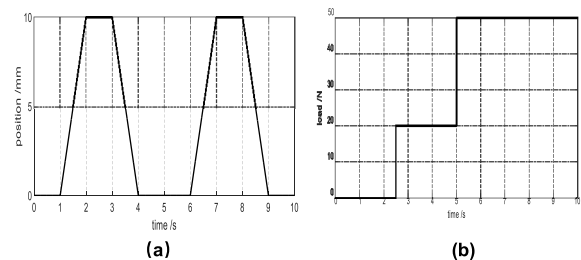


FIGURE 5. (a) Trapezoid reference command (b) External load disturbance.

To guarantee  $\dot{V} \leq 0$ , the sufficient condition being (44) with  $k_1 > \frac{1}{2}$  and  $k_2 > \frac{1}{2}$ . Thus, by Barbalat's Lemma,  $\|z\| \rightarrow 0$  and  $\tilde{\beta}_1 \rightarrow 0$  when  $t \rightarrow \infty$ , which ensures the stability of the system.

In summary, the design steps of the proposed IAJC system is described as follows:

*Step 1:* The filtered error vector, the position tracking error  $e_1$ , the filtered velocity error  $e_2$  and the filtered accelerate error  $e_3$  is calculated as shown in (6) and (7), respectively.

*Step 2:* The control law of the PMLSM servo system is computed by (10).

*Step 3:* The model-based feedforward control law is computed by (11) and the gradient-based adaptive update law is shown in (15).

*Step 4:* The intelligent control law is computed by (18), where the adaptive feedback gain  $\hat{\beta}_1$  is updated by (21).

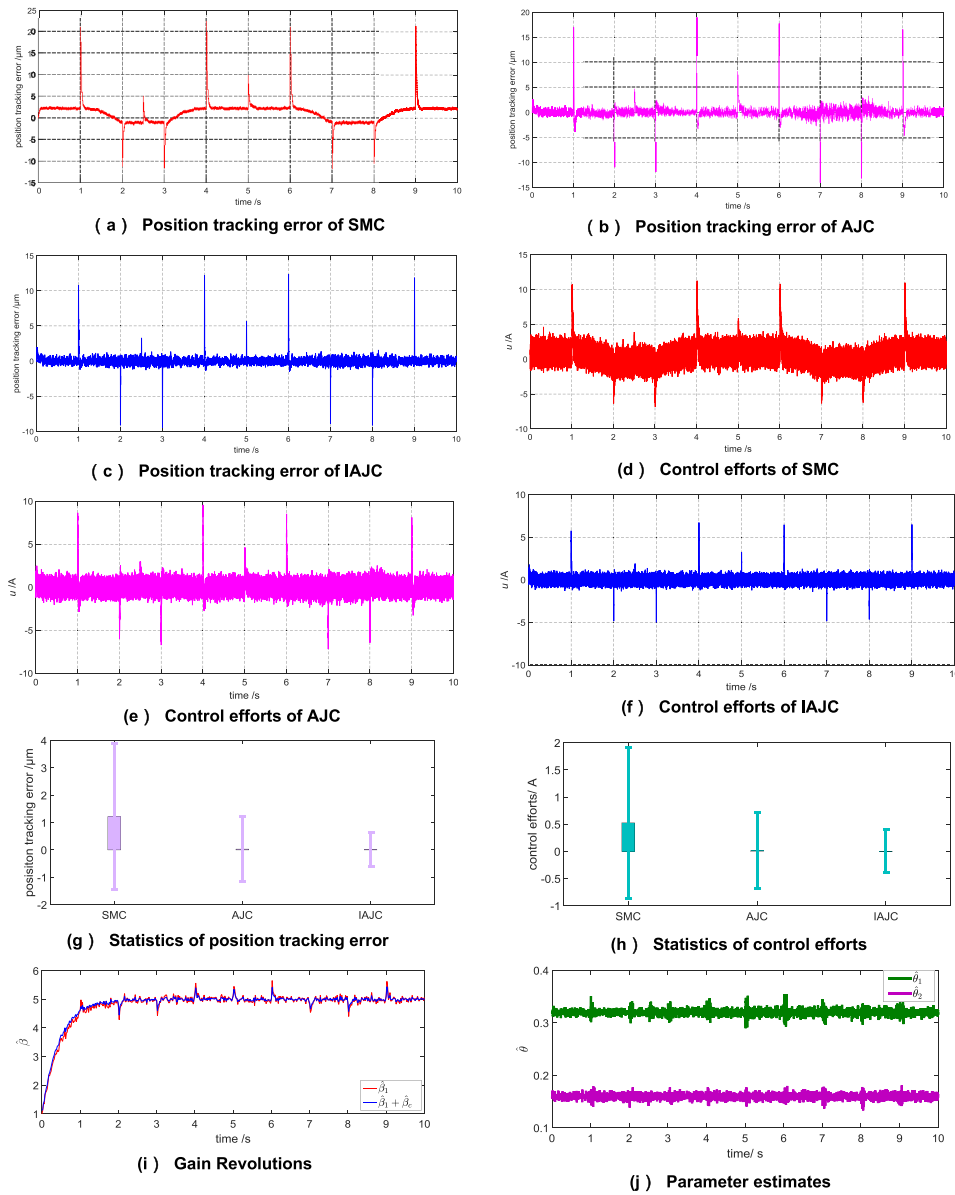


FIGURE 6. Experimental results of trapezoid command.

TABLE 4. Result of RMS position tracking error and control efforts for trapezoid command.

RMS error	Value ( $\mu\text{m}$ )	% change
SMC	2.67	—
AJC	1.19	-59.18%
IAJC	0.62	-76.78%
RMS efforts	Value (A)	% change
SMC	1.3864	—
AJC	0.7015	-49.4%
IAJC	0.3989	-71.2%

Step 5: The input variables of the double-loop RFSFNN are  $e_1$  and  $e_2$ . The output of double-loop RFSFNN, which is

computed by (34), is used to compensate  $\hat{\beta}_1$ . The parameters of double-loop RFSFNN are estimated by the adaptation laws (37) ~ (41).

Step 6: Return to Step 1 and repeat the process.

#### IV. EXPERIMENTAL VERIFICATION

The block diagram of the PMLSM drive system, which consists of a pulsewidth modulated inverter, PI current controllers and a coordinate transformation mechanism of the field-oriented control, is shown in Fig. 3. With the implementation of field-oriented control, the PMLSM system can be directly controlled via (2).

##### A. EXPERIMENTAL SYSTEM

To test the feasibility and the validity of the proposed scheme, DSP-based IAJC for PMLSM servo system is shown in Fig. 4. The parameters of PMLSM are listed in Table 2. The control chip is TMS320F2812A produced by TI. The switching

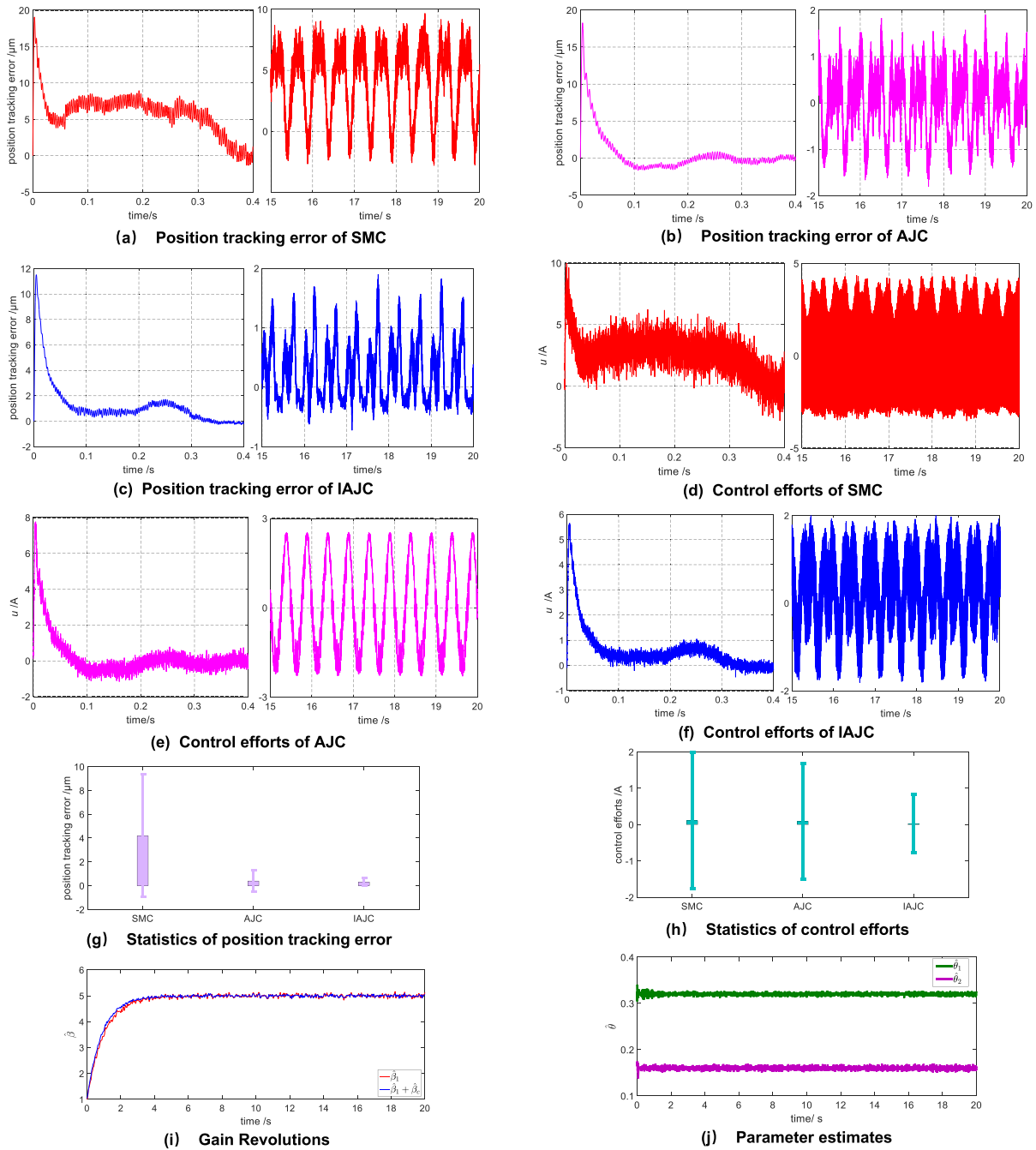


FIGURE 7. Experimental results of sinusoidal command.

frequency of the IPM is 5 kHz. The sampling time of the control system is 200  $\mu$ s.

To illustrate the advantage of intelligent jerk control with the dynamic compensation gain, AJC and SMC with switching law are introduced for comparison. The control law of the SMC is given as

$$u_{SMC} = B_n^{-1} [\ddot{x}_d(t) - A_n \dot{x}(t) + \lambda \dot{e}_1 + \Theta \text{sign}(s/\Phi)] \quad (58)$$

The values of parameters in the above controllers are shown in Table 3. The regulation of the IAJC follows the guidelines provided by Theorem 1.

### B. COMPARATIVE EXPERIMENTS FOR TRAPEZOID COMMAND

For the periodic trapezoid reference command in Fig. 5(a) with the varying external load in Fig. 5(b), it is to validate the effectiveness of the proposed IAJC. Fig. 6 depicts the experimental results of SMC, AJC, and IAJC with dynamic compensation gain.

It can be seen that, concerning the external load disturbance, their performance of position tracking error is shown in Fig. 6(a) ~ (c). Especially, the robust control characteristics can be achieved using the proposed IAJC.

**TABLE 5. Result of RMS position tracking error and control efforts for sinusoidal command.**

RMS error	Value ( $\mu\text{m}$ )	% change
SMC	5.149	—
AJC	0.8775	-82.76%
IAJC	0.7122	-86.17%
RMS efforts	Value (A)	% change
SMC	1.8722	—
AJC	1.5961	-14.75%
IAJC	0.7991	-57.32%

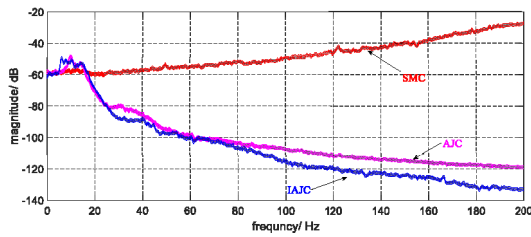
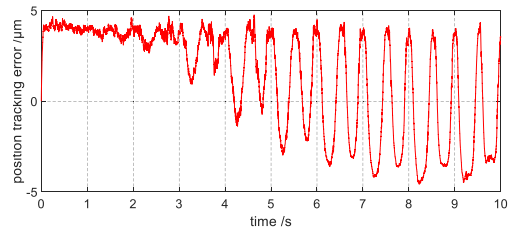


**FIGURE 8. Welch Power Spectral Density estimate of velocity error for sinusoidal command.**

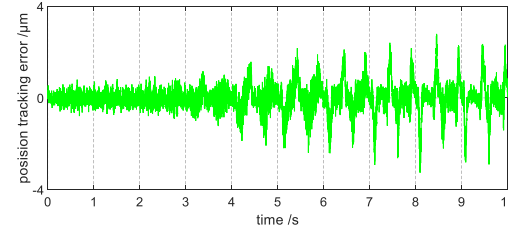
However, the SMC bears larger tracking error at sharp corners, and the tracking performances are evidently deteriorated at a smooth trajectory. Furthermore, as seen in Fig. 6(d) ~ (f), the chattering phenomenon of the SMC is obvious owing to the discontinuous switching law (58). The error distribution statistics of the tracking error and control efforts are shown in Fig. 6(g) ~ (h). Moreover, the root-mean-square (RMS) values of tracking errors and control efforts by three control methods are summarized in Table 4. By comparing the performance between the AJC and the IAJC, it can be known that the dynamic compensation gain of the proposed IAJC can effectively suppress the uncertainties and the chattering phenomenon is attenuated. Although the AJC and the proposed IAJC demonstrate similar tracking performance during the whole tracking performance, it can be seen that, with the help of the dynamic compensation gain, the average and RMS values of the IAJC keep in a small level. The evolutions of the adaptive feedback gain  $\hat{\beta}_1$  and dynamic compensation gain  $\hat{\beta}_c$  are shown in Fig. 6(i). The evolutions are with ripples to cater for the time-varying of the uncertainties.  $\hat{\beta}_1 + \hat{\beta}_c$  is converged following the designed response in the steady-state, which proves the applicability of the exponential adaptive law of  $\hat{\beta}_1$  and the proposed double-loop RFSFNN. The parameter estimates are shown in Fig. 6(j). Here it is evident that the proposed IAJC not only achieved the best robustness and control precision but also eliminated the chattering phenomenon.

**C. COMPARATIVE EXPERIMENTS FOR SINUSOIDAL COMMAND**

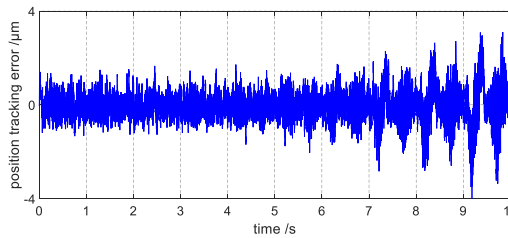
To further verify the tracking performance of the proposed IAJC, the reference command is set as a sinusoidal command



**(a) Position tracking error for  $\beta_1=1$**



**(b) Position tracking error for  $\beta_1=5$**



**(c) Position tracking error for  $\beta_1=9$**

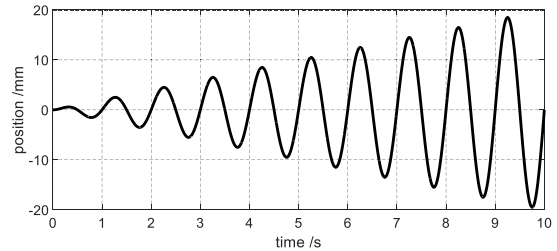


**FIGURE 9. Exponentially increasing sinusoidal reference command.**

described by  $x_d = 0.01\sin(4\pi t)$ . Fig. 7 shows the results of the experiment. The SMC has the worst tracking performance and the position tracking error as a large deviation at the peak of a sinusoidal command, where the velocity nears zero because of the uncertain nonlinear friction in Fig. 7(a). From Fig. 7(b)~(c), the proposed IAJC gives the slower response speed in transient-state, probably due to the adaptation of dynamic compensation gain. Remarkably, it is found that the IAJC system performs the best tracking precision in the long term, as compared with the other control methods. The control efforts of different control methods are presented in Fig. 7(d)~(f). In comparison, the proposed IAJC improves the chattering of control efforts significantly. For the convenience of understanding, the error distribution statistics of tracking error and control effort are shown in Fig. 7(g)~(h). In the meantime, the RMS values of tracking error and control efforts for sinusoidal command are summarized in Table 5. Also, the gain revolutions and parameter estimates are shown in Fig. 7(i)~(j), respectively. Thus, it can be verified that the proposed IAJC can carry out the best control performance

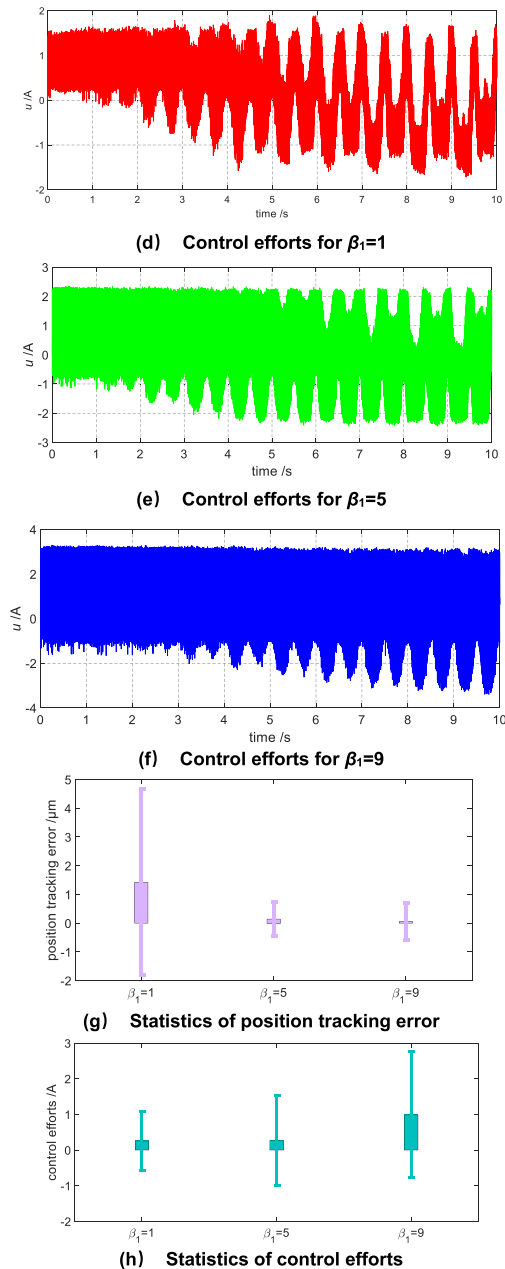


FIGURE 10. Experimental results of different feedback gain.

and is suitable in the tracking control of the PMLSM servo system.

The Welch Power Spectral Density (PSD) estimate of the velocity tracking error for sinusoidal command is shown in Fig. 8. The shaded area represents the 95% confidence bound. It is observed that the PSD of the SMC is larger at the higher frequency because the sign function and the large robust gain cause the SMC to generate chattering phenomenon, which leads to the worse tracking performance. On the contrary, the velocity error of the AJC and the proposed IAJC is concentrated at 0~18Hz, and it is gradually attenuated, which indicates that the continuous control signals, generated by the AJC and the proposed IAJC, do not carry much power at high frequency. Compared with the AJC,

TABLE 6. Result of RMS position tracking error and control efforts for different feedback gain.

RMS error	Value ( $\mu\text{m}$ )
$\beta_1=1$	3.2393
$\beta_1=5$	0.5864
$\beta_1=9$	0.6276
RMS efforts	Value (A)
$\beta_1=1$	0.8169
$\beta_1=5$	1.2662
$\beta_1=9$	1.7698

the proposed IAJC eliminates the chattering phenomenon more effectively at high frequency. Hence, the control efforts of IAJC will not excite high-order terms in unmodeled dynamics, which means that high-frequency oscillation can be avoided.

D. EFFECT OF DIFFERENT FEEDBACK GAIN  $\beta_1$

To investigate the effect of different feedback gain  $\beta_1$  of the proposed IAJC, in this experimental test, an exponentially increasing sinusoidal reference command is given in Fig. 9, and the experimental results of variable robust gain are shown in Fig. 10. To show compensation results clearly, Table 6 gives the RMS values of position tracking error and control efforts under different values of feedback gain  $\beta_1$ .

The reference command is difficult to be tracked at the initial time since the velocity of this trajectory is rather small, the nonlinear friction force centralizes in the Stribeck effect area. From these compensation results, it is found that there is an optimal choice to set the feedback gain  $\beta_1 = 5$ . When the value of  $\beta_1$  is equals to 1, the position tracking error is larger, especially in the initial time. Meanwhile, the chattering phenomenon of the control effects is limited in a rational range. Although the tracking error is convergence in the steady-state, when  $\beta_1 = 9$ , it is difficult to obtain satisfactory control performance due to the chatting phenomenon. It is predictive that the larger value of  $\beta_1$  leads to an increased jerk, which makes the proposed method is similar to the SMC with discontinuous control law. On the contrary, if the value of  $\beta_1$  is selected to be 1, it is too small to cater to the uncertainties of the system so that the tracking performance is worse. Based on the above-mentioned results, it is suggested that an appropriate selection of feedback gain  $\beta_1$  will improve the tracking performance of the system without adding significant cost in control effort.

V. CONCLUSION

This paper proposed an IAJC scheme with dynamic compensation gain for the PMLSM servo system to achieve high-precision and high-velocity control performance, which guaranteed the robustness in the presence of the external load disturbance, parametric uncertainties, nonlinear friction, and unmodeled dynamics. To generate stable and continuous

control efforts to improve the control performance of the PMLSM servo system, the AJC was proposed and the exponential update law guaranteed bounded adaptive feedback gain of the jerk. Additionally, to compensate for the approximation deviation and attenuate the chattering phenomenon, a dynamic compensation gain was designed by the double-loop RFSFNN. The double-loop structure can enhance the approximation performance of the RFNN and the feature selection mechanism can eliminate the unfavorable features to improve the learning capability of the FNN. The stability of the closed-loop system was proved by the Lyapunov approach. The experimental results verify robustness and tracking performance of the proposed IAJC with respect to the PMLSM servo system.

## REFERENCES

- [1] F.-J. Lin, L.-T. Teng, and H. Chu, "A robust recurrent wavelet neural network controller with improved particle swarm optimization for linear synchronous motor drive," *IEEE Trans. Power Electron.*, vol. 23, no. 6, pp. 3067–3078, Nov. 2008.
- [2] C.-S. Ting, J.-F. Lieu, C.-S. Liu, and R.-W. Hsu, "An adaptive FNN control design of PMLSM in stationary reference frame," *J. Control, Autom. Electr. Syst.*, vol. 27, no. 4, pp. 391–405, Apr. 2016.
- [3] F. Wang, C. Liang, Y. Tian, X. Zhao, and D. Zhang, "A flexure-based kinematically decoupled micropositioning stage with a centimeter range dedicated to micro/nano manufacturing," *IEEE/ASME Trans. Mechatronics*, vol. 21, no. 2, pp. 1055–1062, Apr. 2016.
- [4] T. H. Liu, Y. C. Lee, and Y. H. Chang, "Adaptive controller design for a linear motor control system," *IEEE Trans. Aerosp. Electron. Syst.*, vol. 40, no. 2, pp. 601–613, Apr. 2004.
- [5] J. Yao, Z. Jiao, and B. Yao, "Robust control for static loading of electrohydraulic load simulator with friction compensation," *Chin. J. Aeronaut.*, vol. 25, no. 6, pp. 954–962, Dec. 2012.
- [6] J.-C. Shen, Q.-Z. Lu, C.-H. Wu, and W.-Y. Jywe, "Sliding-mode tracking control with DNLRX model-based friction compensation for the precision stage," *IEEE/ASME Trans. Mechatronics*, vol. 19, no. 2, pp. 788–797, Apr. 2014.
- [7] K. Cho, J. Kim, S. B. Choi, and S. Oh, "A high-precision motion control based on a periodic adaptive disturbance observer in a PMLSM," *IEEE/ASME Trans. Mechatronics*, vol. 20, no. 5, pp. 2158–2171, Oct. 2015.
- [8] S.-L. Chen, K. Kiong Tan, and S. Huang, "Friction modeling and compensation of servomechanical systems with dual-relay feedback approach," *IEEE Trans. Control Syst. Technol.*, vol. 17, no. 6, pp. 1295–1305, Nov. 2009.
- [9] K. K. Tan, T. H. Lee, S. N. Huang, and X. Jiang, "Friction modeling and adaptive compensation using a relay feedback approach," *IEEE Trans. Ind. Electron.*, vol. 48, no. 1, pp. 169–176, Feb. 2001.
- [10] M. Y. Wei and T. H. Liu, "Design and implementation of an online tuning adaptive controller for synchronous reluctance motor drives," *IEEE Trans. Ind. Electron.*, vol. 60, no. 9, pp. 3644–3657, Sep. 2013.
- [11] K. Y. Chen, "Sliding mode minimum-energy control for a mechatronic motor-table system," *IEEE/ASME Trans. Mechatronics*, vol. 21, no. 3, pp. 1487–1495, Jun. 2016.
- [12] M. A. M. Cheema, J. E. Fletcher, M. Farshadnia, D. Xiao, and M. F. Rahman, "Combined speed and direct thrust force control of linear permanent-magnet synchronous motors with sensorless speed estimation using a sliding-mode control with integral action," *IEEE Trans. Ind. Electron.*, vol. 64, no. 5, pp. 3489–3501, May 2017.
- [13] J. P. Su and C. C. Wang, "Complementary sliding control of non-linear system," *Int. J. Control*, vol. 75, no. 5, pp. 360–368, Mar. 2002.
- [14] B. Beltran, T. Ahmed-Ali, and M. Benbouzid, "High-order sliding-mode control of variable-speed wind turbines," *IEEE Trans. Ind. Electron.*, vol. 56, no. 9, pp. 3314–3321, Sep. 2009.
- [15] H. M. Chen, J. P. Su, and J. C. Renn, "A novel sliding mode control of an electrohydraulic position servo system," *IEICE Trans. Fundam. Electron. Commun. Comput. Sci.*, vol. E85-A, no. 8, pp. 1928–1936, 2002.
- [16] F.-J. Lin, J.-C. Hwang, P.-H. Chou, and Y.-C. Hung, "FPGA-based intelligent-complementary sliding-mode control for PMLSM servo-drive system," *IEEE Trans. Power Electron.*, vol. 25, no. 10, pp. 2573–2587, Oct. 2010.
- [17] F. Wang, C. Liang, Y. Tian, X. Zhao, and D. Zhang, "Design and control of a compliant microgripper with a large amplification ratio for high-speed micro manipulation," *IEEE/ASME Trans. Mechatronics*, vol. 21, no. 3, pp. 1262–1271, Jun. 2016.
- [18] S. Ebrahimkhani, "Robust fractional order sliding mode control of doubly-fed induction generator (DFIG)-based wind turbines," *ISA Trans.*, vol. 63, pp. 343–354, Jul. 2016.
- [19] Z. Cai, M. S. deQueiroz, and D. M. Dawson, "Robust adaptive asymptotic tracking of nonlinear systems with additive disturbance," *IEEE Trans. Autom. Control*, vol. 51, no. 3, pp. 524–529, Mar. 2006.
- [20] P. M. Patre, W. MacKunis, C. Makkar, and W. E. Dixon, "Asymptotic tracking for systems with structured and unstructured uncertainties," *IEEE Trans. Control Syst. Technol.*, vol. 16, no. 2, pp. 373–379, Mar. 2008.
- [21] J. Shin, H. J. Kim, Y. Kim, and W. E. Dixon, "Autonomous flight of the rotorcraft-based UAV using RISE feedback and NN feedforward terms," *IEEE Trans. Control Syst. Technol.*, vol. 20, no. 5, pp. 1392–1399, Sep. 2012.
- [22] Z. Yao, J. Yao, and W. Sun, "Adaptive RISE control of hydraulic systems with multilayer neural-networks," *IEEE Trans. Ind. Electron.*, vol. 66, no. 11, pp. 8638–8647, Nov. 2019.
- [23] B. Xian, D. M. Dawson, M. S. de Queiroz, and J. Chen, "A continuous asymptotic tracking control strategy for uncertain nonlinear systems," *IEEE Trans. Autom. Control*, vol. 49, no. 7, pp. 1206–1211, Jul. 2004.
- [24] P. M. Patre, W. MacKunis, K. Dupree, and W. E. Dixon, "Modular adaptive control of uncertain Euler–Lagrange systems with additive disturbances," *IEEE Trans. Autom. Control*, vol. 56, no. 1, pp. 155–160, Jan. 2011.
- [25] J. Yao, Z. Jiao, and D. Ma, "RISE-based precision motion control of DC motors with continuous friction compensation," *IEEE Trans. Ind. Electron.*, vol. 61, no. 12, pp. 7067–7075, Dec. 2014.
- [26] P. M. Patre, W. MacKunis, K. Kaiser, and W. E. Dixon, "Asymptotic tracking for uncertain dynamic systems via a multilayer neural network feedforward and RISE feedback control structure," *IEEE Trans. Autom. Control*, vol. 53, no. 9, pp. 2180–2185, Oct. 2008.
- [27] J. Yao, W. Deng, and Z. Jiao, "RISE-based adaptive control of hydraulic systems with asymptotic tracking," *IEEE Trans. Autom. Sci. Eng.*, vol. 14, no. 3, pp. 1524–1531, Jul. 2017.
- [28] B. Bidikli, E. Tatlicioglu, and E. Zergeroglu, "A self tuning RISE controller formulation," in *Proc. Amer. Control Conf. (ACC)*, Portland, OR, USA, Jun. 2014, pp. 5608–5613.
- [29] S.-Y. Chen and T.-S. Liu, "Intelligent tracking control of a PMLSM using self-evolving probabilistic fuzzy neural network," *IET Electr. Power Appl.*, vol. 11, no. 6, pp. 1043–1054, Jul. 2017.
- [30] H.-H. Chiang, K.-C. Hsu, and I.-H. Li, "Optimized adaptive motion control through an SoPC implementation for linear induction motor drives," *IEEE/ASME Trans. Mechatronics*, vol. 20, no. 1, pp. 348–360, Feb. 2015.
- [31] F.-J. Lin, S.-Y. Chen, L.-T. Teng, and H. Chu, "Recurrent functional-link-based fuzzy neural network controller with improved particle swarm optimization for a linear synchronous motor drive," *IEEE Trans. Magn.*, vol. 45, no. 8, pp. 3151–3165, Aug. 2009.
- [32] F. F. M. El-Sousy and K. A. Abuhasel, "Self-organizing recurrent fuzzy wavelet neural network-based mixed  $H_2/H_\infty$  adaptive tracking control for uncertain two-axis motion control system," *IEEE Trans. Ind. Appl.*, vol. 52, no. 6, pp. 5139–5155, Nov./Dec. 2016.
- [33] J.-X. Peng, K. Li, and D.-S. Huang, "A hybrid forward algorithm for RBF neural network construction," *IEEE Trans. Neural Netw.*, vol. 17, no. 6, pp. 1439–1451, Nov. 2006.
- [34] F.-J. Lin, I.-F. Sun, K.-J. Yang, and J.-K. Chang, "Recurrent fuzzy neural cerebellar model articulation network fault-tolerant control of six-phase permanent magnet synchronous motor position servo drive," *IEEE Trans. Fuzzy Syst.*, vol. 24, no. 1, pp. 153–167, Feb. 2016.
- [35] R. Chakraborty and N. R. Pal, "Feature selection using a neural framework with controlled redundancy," *IEEE Trans. Neural Netw. Learn. Syst.*, vol. 26, no. 1, pp. 35–50, Jan. 2015.
- [36] C.-T. Lin, N. R. Pal, S.-L. Wu, Y.-T. Liu, and Y.-Y. Lin, "An interval type-2 neural fuzzy system for online system identification and feature elimination," *IEEE Trans. Neural Netw. Learn. Syst.*, vol. 26, no. 7, pp. 1442–1455, Jul. 2015.

- [37] Q. Yang, S. Jagannathan, and Y. Sun, "NN/RISE-based asymptotic tracking control of uncertain nonlinear systems," in *Proc. Int. Symp. Intell. Control IEEE Multi-Conf. Syst. Control*, Denver, CO, USA, Sep. 2011, pp. 1361–1366.



**HAO YUAN** was born in Dalian, China, in 1992. He received the B.S. degree from the Qingdao University of Technology, Qingdao, China, in 2014, and the M.S. degree in electrical engineering from the Shenyang University of Technology, Shenyang, China, in 2019, where he is currently pursuing the Ph.D. degree in electrical engineering.

His current research interests include the design of PMLSM servo systems, coordinated synchronization control of multi-axis servo systems, intelligent control, nonlinear and robust control, and precision motion control.



**XIMEI ZHAO** was born in Changchun, Jilin, China, in 1979. She received the B.S., M.S., and Ph.D. degrees in electrical engineering from the Shenyang University of Technology, Shenyang, China, in 2003, 2006, and 2009, respectively. She is currently a Professor and a Ph.D. Supervisor with the School of Electrical Engineering, Shenyang University of Technology. Her research interests include electrical machines, motor drives, motor control, intelligent control, and robot control. She has authored or coauthored more than 100 technical articles, three textbooks, and holds 15 patents in these areas.



**DONGXUE FU** received the B.S. degree in electrical engineering and automation from Beihua University, Jilin, China, in 2017. He is currently pursuing the Ph.D. degree with the School of Electrical Engineering, Shenyang University of Technology. His current research interests include motor control, intelligent control, and neural networks.

...